Journal of Hydrology: Regional Studies 59 (2025) 102399

Contents lists available at ScienceDirect

Journal of Hydrology: Regional Studies

journal homepage: www.elsevier.com/locate/ejrh

Increased intensity and frequency of extreme precipitation events in Belgium as simulated by the regional climate model MAR

Josip Brajkovic [a,*], Xavier Fettweis [a], Brice Noël [a], Hans Van De Vyver [b], Nicolas Ghilain [a,b], Pierre Archambeau [c], Michel Pirotton [c], Sébastien Doutreloup [a]

[a] Department of Geography, Laboratory of Climatology and Topoclimatology, SPHERES, University of Liege, Liege, Belgium
[b] Royal Meteorological Institute, RMI, Uccle, Belgium
[c] Department of Environmental Engineering, University of Liege, Liege, Belgium

ARTICLE INFO

Keywords:
Extreme precipitation
Extreme value analysis
MAR
Global warming
Belgium

ABSTRACT

Study region: Belgium
Study focus: In July 2021, Western Germany, the Netherlands and Belgium were hit by extreme rainfall events of unprecedented intensity, raising concerns about future trends. To assess future trends in extreme precipitation frequency and intensity, we use the regional climate model MAR at 5-km spatial resolution to conduct climate projections until 2100. MAR is forced by a set of six CMIP6 Earth System model (ESMs) with 4 IPCC scenarios ranging from low to high-end warming.
Study insights: First, an Extreme Value Analysis (EVA) is performed on bias-adjusted daily model outputs over 30-year moving windows. We find that, on average, extreme precipitation intensity rises following the Clausius-Clapeyron scaling, i.e., a 7% increase per additional degree of global warming. This trend results from a clear increase in the spread and in the modes of the extreme precipitation event distributions. Second, an EVA is performed over the complete simulated period (2015-2100). Our analyses reveal that, even under low-warming scenarios, return level maps, i.e., representing the precipitation values associated with a certain return period, are more intense than those obtained using observational data over 1951-2021. For the 21st century, the 20-year daily return level can locally reach 100 mm per day, which represents a 25%–30% increase relative to the present day.

1. Introduction

The rainfall event of July 2021 which caused major floods over western Germany, Belgium and the Netherlands was of unprecedented intensity. The amount of cumulated precipitation over 3 days (i.e., 14th to 16th of July) reached 290 mm in the basin of the Vesdre valley (purple contour in Fig. 1a) (Journée et al., 2023), accounting for approximately 20% of the annual mean precipitation over High Belgium (Erpicum et al., 2017) (Fig. 1). Belgium's topography generally follows a northwestern-southeastern gradient with its highest parts located in the Ardennian Massif near the German border (purple contour in Fig. 1b). Usually, we distinguish three topographic areas: Low Belgium (0–100 m), Medium Belgium (100–300 m) and High Belgium (above 300 m) (Fig. 1). Over Medium and Low Belgium, annual precipitation average ranges from 600 to 800 mm with a 1300 mm peak for the highest parts of Belgium. Dominant Westward Circulation patterns explain this precipitation pattern, exhibiting relatively low values for an oceanic type climate (Erpicum et al., 2017).

* Corresponding author.
E-mail address: josip.brajkovic@uliege.be (J. Brajkovic).

https://doi.org/10.1016/j.ejrh.2025.102399
Received 10 September 2024; Received in revised form 1 April 2025; Accepted 11 April 2025
Available online 9 May 2025
2214-5818/© 2025 Published by Elsevier B.V. This is an open access article under the CC BY-NC-ND license (http://creativecommons.org/licenses/by-nc-nd/4.0/).

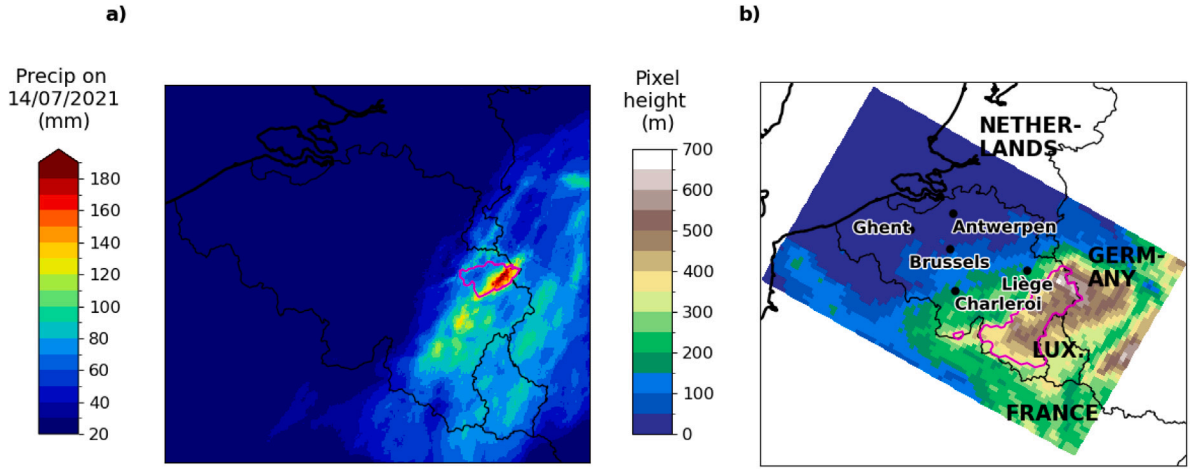

Fig. 1. (a) Precipitation on the 14th of July 2021 as recorded by the radar (Journée et al. 2021). The catchment of the Vesdre river is highlighted in purple. (b) MAR inner domain topography at 5 km. The Ardennian Massif is located in Belgium and highlighted in purple.

Table 1
ESMs used to force MAR at its lateral boundaries (modified after (Sobolowski et al., 2023)). TCR = Transient Climate Response.

CMIP6 ESM	Member	TCR Plausible range (1.2K-2.4K)	Name in this paper
MIROC6	r1ip1f1	1.55	MAR-MIR
NorESM2-MM	r1ip1f1	1.33	MAR-NS2
MPI-ESM-2-HR	r1ip1f1	1.66	MAR-MPI
EC-Earth3-Veg-HR	r1ip1f1	2.62	MAR-EC3
CMCC-CM2-SR5	r1ip1f1	2.09	MAR-CR5
IPSL-CM6A-LR	r1ip1f1	2.32	MAR-IPSL

In July 2021, the Vesdre valley experienced strong floods resulting from extreme precipitation, with major damages to human infrastructures (Dewals et al., 2021) (Fig. 1a). Recent analyses attributed a 400-year return period to this extreme precipitation event (Tradowsky et al., 2023), which was linked to a very singular meteorological situation, with at least three aggravating factors.

At the synoptic scale, the meteorological situation was driven by a depression centered over Germany with an associated North-East flux over Belgium. On top of this, a quasi-stationary rainy occluded front stagnated over the whole Vesdre valley for three consecutive days, constituting a first aggravating factor. A second factor was related to the depression typology: a cut-off low with an associated cold core. That cold air, which was at middle altitudes (about 5 kilometers), enhanced the precipitation production by allowing ascending convective movements into the air mass, hence leading to rapid moist condensation. The depression was also unstable which favored the formation of embedded convective precipitation. A third factor lies in the topography of the Ardennian Massif (Fig. 1b) which "barrier effect" played a key role in forcing the air mass to rise, in turn enhancing condensation and subsequent precipitation (ECMWF, 2021).

In a context of global warming, it is crucial to determine whether such events become more frequent and more intense in the near future. At the global scale, the predicted precipitation change varies spatially but the frequency of more intense events is expected to increase (IPCC, 2023b). The rarer the event the higher the increase in intensity (Gründemann et al., 2022; Pfahl et al., 2017). Hence, the 100-year return period for 1-day rainfall intensity is expected to raise by 13.5 to 38.3% for low and high emissions scenarios, respectively. However, for the Western Central Europe region, while the observed change in heavy precipitation shows an increase, the confidence in the anthropogenic contribution remains low (IPCC, 2023a). At the European scale, for Summer, EURO-CORDEX Regional Climate Models (RCMs) ensemble simulations show a drying of the Mediterranean area while Northern Europe experiences wetter conditions with trends being more pronounced for high emission scenarios (Rajczak and Schär, 2017). For extreme events with return periods ranging from 10 to 100 years, the increase in intensity varies from 15 to 35% in Northwestern Europe by 2070–2099 for the AR5 RCP8.5 scenario.

The impact of global warming on extreme precipitation has been studied in various countries (Babaousmail et al., 2022; Kendon et al., 2023; Luppichini et al., 2023; Arnbjerg-Nielsen, 2012). However, in Belgium, only a few studies have assessed these impacts of climate change (de Vyver et al., 2021; Muñoz Lopez et al., 2023). For instance, Hosseinzadehtalaei et al. (2018) analyzed the outputs of the Euro-Cordex community members to explore the response of Intensity Duration Frequency curves (IDFs) to Global Warming at specific locations. Their results suggest that the 10-year return level of daily rainfall might increase by 50 to 70% under a RCP8.5 scenario for Central Belgium.

Kreienkamp et al. (2021) attributed the July 2021 event by computing trends in extreme precipitation distributions shapes. Their results suggest that the occurrence of the 2021 large scale event has become 1.2 to 9 times more likely due to climate change.

Although the return period is estimated at 400 years based on observations, its frequency is expected to further increase with additional global warming. The findings of Mohr et al. (2023) and Ludwig et al. (2023) showed the July 2021 rainfall event could have even been 7 to 9% more intense per degree of added global warming. Using a storyline approach, they concluded that this event was 11% more intense than it would have been under pre-industrial conditions.

In this paper, we use climate projections from one high-resolution Regional Climate Model (RCM) called MAR (Modèle Atmosphérique Régional) to estimate future trends in extreme precipitation events intensity and frequency across Belgium, and quantify their intensity within the 21st century. First, using the Extreme Value Analysis (EVA) theory, we look at future daily extreme precipitation anomalies over 30-year periods (Section 3.1). Then, the whole simulated period (2015–2100) is used to compute absolute values of extreme precipitation associated to particular return periods, hereafter referred to as return levels (Section 3.2). Finally, we discuss the methodological choices and the major limitations of the conducted analyses (Section 4).

2. Material and method

2.1. The MAR model

Here we use the *Modèle Atmosphérique Régional* (MAR) at high spatial resolution (5-km, Fig. 1) to locally explore the impact of global warming on extreme precipitation frequency and intensity.

MAR is a hydrostatic regional climate model (RCM) solving primitive equations (Gallée and Schayes, 1994a), which has been thoroughly evaluated over Belgium for both temperatures (Doutreloup et al., 2022b,a) and precipitation (Doutreloup et al., 2019). For precipitation, special attention has been drawn to events linked to floods over the Ourthe catchment (Wyard et al., 2021) and to more specific meteorological events such as freezing rain Fettweis et al. (2017). MAR's convection is parameterized after (Bechtold et al., 2001; Doutreloup et al., 2019). Its atmospheric part is described in Gallée and Schayes (1994b) and Gallée (1995). MAR is coupled with the Soil Ice Snow Vegetation Atmosphere Transfer model (SISVAT) which represents the interactions between the surface and the atmosphere, the percolation of water in the soil and surface run-off (Wyard et al., 2017). Here, we use the latest MAR version 3.14 (Grailet et al., 2024). MAR domain (Fig. 1) is rotated for computational efficiency purposes and to cover Belgium, parts of Western Germany, Northern France, the Netherlands and Luxembourg within a same grid.

Over the present climate (1940–2021), MAR was forced by ERA5 reanalyses (MAR-ERA5) and was evaluated using observational data from the Belgian Royal Meteorological Institute (RMI). For climate projections, MAR was forced by six CMIP6 community members (Table 1) using a single nesting procedure. Control runs (1980–2014) were first compared to MAR outputs and observations over their overlapping period. By doing so, we assessed the performance of MAR outputs, ensuring their ability to be used as input of Extreme Value Analyses (EVA) (Table 2). The six CMIP6 Earth System Models (ESMs) members (Table 1) forcing MAR were selected following the recommendations of the Euro-Cordex community (Sobolowski et al., 2023). The used ESMs have different climate sensitivities as highlighted by their Transient Climate Responses (TCR). The TCR can be defined as the Global Warming Level (GWL) reached by the ESM for a doubling of the initial CO_2 concentration, with the CO_2 being added in the atmosphere at a constant rate (IPCC, 2023b). Four Shared Socioeconomic Pathways baseline scenarios (SSP) are used ranging from low-end (SSP1-2.6) to high-end emissions (SSP5-8.5) (see Fig. 3 for the Global Mean Surface Temperature (GMST) anomaly reached under specific scenarios for all the models).

2.2. Statistical methodology

Here, we use two common approaches in EVA, namely the Annual Maxima (AM) and Peaks Over Threshold (POT) to assess the robustness of our methodology. These two approaches fit stationary laws (GEV and GPD respectively) to the studied samples, i.e, where parameters do not vary with time. The results of this paper focus on the POT approach since both approaches yield close results (see discussion Section 4.1.1).

2.2.1. Peaks Over Threshold (POT) approach

The Peaks Over Threshold (POT) approach fits a General Pareto Distribution (GPD) to threshold exceedances. Selecting values exceeding a given precipitation threshold u yields a larger sample size with more information about the distribution of high precipitation events. To ensure that all the selected events are statistically independent, clusters must be identified in the sample. A cluster is defined as a group of events (one event or more) separated by a period of time shorter than a given number of days (Coles, 2001). For this study, it was set to 7 days (one week) which is an arbitrary choice. However, one week seems to be a reasonable value for selecting events that are caused by independent synoptic patterns.

When all the clusters have been identified, only the highest values of the clusters (i.e., exceeding threshold u) are conserved in the sample. Here, we set this threshold to the 99.5 th quantile of the daily rainfall (including dry days). This value was chosen because it fulfills the requirement of having an average value of selected events per year $\lambda > 2$. The latter requirement confers an advantage to the POT over the AM method, which is based on one selected event per year (Grandry et al., 2020; Cunnane, 1979; Taesombut et al., 1978). The impact of the threshold choice is further discussed in Section 4.1.2. The GPD has two parameters σ and ξ which are respectively the scale parameter and the shape parameter. The σ parameter affects the spread of the distribution and ξ influences the weight of the distribution tail (Supplemantary Figure S1a displays the impacts of those parameters on the GPD

Table 2
Statistical parameters computed spatially over Belgium over the control period 1981–2010 : Mean value, standard deviation (std), mean bias (MB), Random Mean Square Error (RMSE) and determination coefficient (r^2) for the 2-year and 20-year return levels (duration = 24 h) over Belgium (spatial statistics). Units for mean, std, MB and RMSE are mm.hour^{-1}. MB and RMSE are computed using the difference between the observed return levels and the simulated ones for all the pixels within Belgium.

models	2-year return level						20-year return level					
	Mean	std	MB	MB (%)	RMSE	r^2	Mean	std	MB	MB (%)	RMSE	r^2
Obs	1.7	0.2	0.0	0.0	0.00	1.00	2.9	0.4	0.0	0.0	0.00	1.00
MAR-ERA5	1.2	0.2	−0.5	−30.5	0.54	0.74	2.0	0.3	−0.8	−29.7	0.92	0.48
MAR-MPI	1.1	0.2	−0.6	−36.0	0.63	0.68	1.7	0.2	−1.1	−40.2	1.22	0.09
MAR-EC3	1.1	0.2	−0.6	−34.9	0.61	0.79	1.8	0.3	−1.1	−38.7	1.20	0.04
MAR-MIR	1.2	0.2	−0.5	−27.6	0.51	0.61	2.1	0.3	−0.7	−25.9	0.86	0.26
MAR-NS2	1.3	0.2	−0.4	−25.9	0.47	0.70	2.0	0.3	−0.8	−29.7	0.94	0.20
MAR-CR5	1.4	0.2	−0.4	−20.9	0.39	0.69	2.2	0.3	−0.6	−22.5	0.74	0.44
MAR-IPSL	1.1	0.2	−0.6	−37.7	0.66	0.68	1.7	0.3	−1.1	−39.0	1.22	0.03

Probability Density Function (PDF)). After the fitting, the return level associated to a return period of T years R_T can be obtained following (Coles, 2001):

$$R_T = \begin{cases} u + \frac{\sigma}{\xi}(\lambda T)^{\xi-1} & \text{, for } \xi \neq 0 \\ u + \sigma log(\lambda T) & \text{, for } \xi = 0 \end{cases} \quad (1)$$

Here u and λ represent, respectively, the chosen threshold value and the mean number of clusters exceeding the threshold each year.

The fitting of the EVA statistical laws are performed by Maximum Likelihood Estimation (MLE) using the R package *ismev* (Gilleland, 2003).

2.2.2. Representation of extremes in MAR

Over Belgium, using observational data from the control period 1981–2010, the GPD-derived 24-hour 2 and 10-year return levels reach intensities of up to 1.7 and 2.8 mm.hour^{-1} (Table 2). The mean bias of MAR-ERA5 for different return levels is on average around -30%. However, when MAR is forced by CMIP6 ESMs, the mean bias increases (about 35% for MAR-EC3, MAR-MPI and MAR-IPSL) or decreases in some cases (around 21% for MAR-CR5). The ability of MAR to correctly represent extreme precipitation events seems to rely on the forcing ESMs ability to create synoptic extreme weather patterns at the domain boundaries. Since the occurrence of such patterns is partly stochastic and depends on the internal variability of the ESMs over the study area (Jain et al., 2023; Kendon et al., 2023), for higher return levels (e.g. 20 years), spatial correlation coefficients (r^2) can drop to 0.03 (MAR-EC3).

Those biases illustrate the need for bias-adjustment of MAR outputs. Here, the observations used for MAR outputs correction consist in gridded daily precipitation data from the Royal Meteorological Institute (RMI) covering the period 1950–2021 at a resolution of 5 km (Journée et al., 2023).

The bias-adjustment procedure used to correct the sampled values is based on the distributions of the POT (i.e., u = 99.5th quantile of the daily precipitation time-series) over the period 1981–2010. Bias-adjustment consists in matching the simulated quantiles to the observed ones. This technique is referred to as Equidistant quantile matching (EDCDFm) (Pierce et al., 2015).

Projected precipitation values V_{sim} are corrected using a multiplicative change factor CF. To calculate this factor, the position of V_{sim} in the simulated Cumulative Density Function (CDF) must be retrieved. This requires to identify the two empirical quantiles $q_{sim,i}$ and $q_{sim,i+1}$ with $q_{sim,i} < V_{sim} < q_{sim,i+1}$. Then, CF is computed using the observed quantiles of the control period (1981–2010) $q_{obs,i}$ and $q_{obs,i+1}$, and the quantiles of the simulated daily precipitation over the control period $q_{cont,i}$ and $q_{cont,i+1}$:

$$CF = [\frac{q_{obs,i}}{q_{cont,i}} * W_i + \frac{q_{obs,i+1}}{q_{cont,i+1}} * W_{i+1}] - 1 \quad (2)$$

where W_i and W_{i+1} represent weights which are computed as follows:

$$W_i = 1 - \frac{V_{sim} - q_{sim,i}}{q_{sim,i+1} - q_{sim,i}} > 0 \quad (3)$$

CF can reach 50% on the coast of Belgium where MAR struggles at representing extreme precipitation. Over regions with steeper topographic gradients, its performance increases with lower CF values down to 15% (Fig. 2).

To avoid abrupt changes over short distances in the return level maps, which might not be representative of the reality, all pixel values shown in maps hereafter have been smoothed using a 3 by 3 averaging kernel, which is an arbitrary choice.

3. Results

3.1. Linking extreme precipitation anomalies to global warming (working on 30-year periods)

The distributions of extreme events are overall shifting towards more extreme values. Firstly, the modes of the extremes are increasing, as shown by the rise of the threshold u (99.5th quantile) in the POT approach (Fig. 3a). This parameter displays an

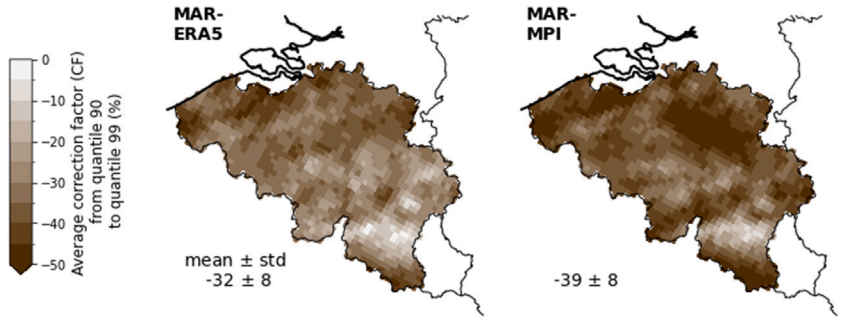

Fig. 2. Average Correction Factor (CF) from quantile 90 to quantile 99 of the POT (Peaks over Threshold) for two selected models ((a) MAR-ERA5 and (b) MAR-MPI). Other models are displayed in Supplementary Figure S3.

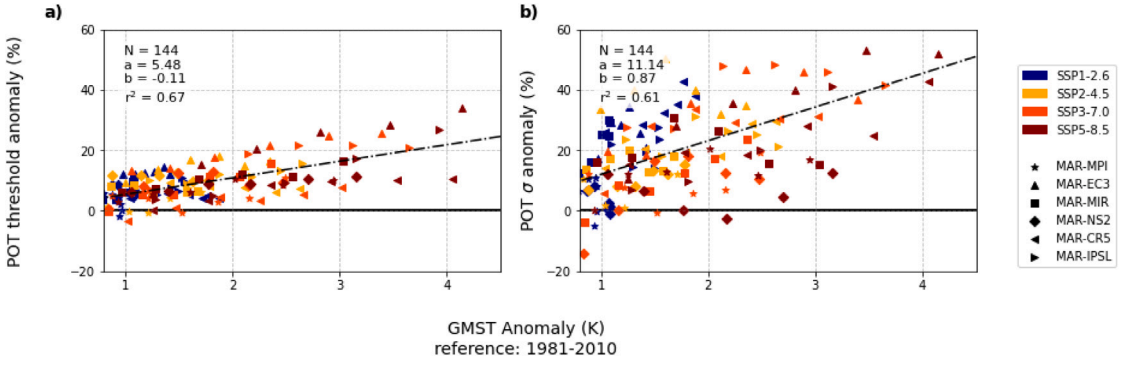

Fig. 3. Anomalies relative to 1981–2010 averaged over 30-year moving windows (from 2021–2050 to 2071–2100 with a 10-year time-step) for (a) POT threshold, (b) GPD-derived σ. A linear regression is applied to the data clouds (black dotted line of slope a and intercept b). The impact of those parameters on the PDFs is displayed in Supplementary Material Fig. S1. The GMST anomaly reached for each model is plotted on Supplementary Material Fig. S2.

increases of 5.5%K^{-1} of additional global warming respectively. This trend value is obtained by fitting a linear regression on the spatially averaged future anomalies over 30-year periods (slope a on Fig. 3a). Those periods are obtained by moving a 30-year window from 2021–2050 to 2071–2090. This leads to point clouds of 6 (30-year periods) x 4 (scenarios) x 6 (models) = 144 points. Second, the spread of the extremes becomes larger. This is clearly shown by the increase of the σ parameter, with a trends reaching 11%K^{-1} (Fig. 3b).

This results in an average increase of 7%K^{-1} of additional global warming for various return levels, in line with the Clausius-Clapeyron scaling (CC-scaling) (Fig. 4a), i.e., a 7% raise in atmospheric moisture for each K of warming (Trenberth et al., 2003). However, we find that, despite having an overall averaged increasing trend of 7 %K^{-1} irrespective of the return period, the correlation to global warming is greater for smaller return periods (Fig. 4a). Hence, we assume that this fluctuation stems from the internal variability of the ESMs. Indeed, due to the natural variability within the Earth system, the periods with the most extreme and rarest events might not be the warmest ones (Kendon et al., 2023; Jain et al., 2023) and thus not the latest ones. For some ESMs under a particular scenario, most extreme events (above 150 mm per day after bias-adjustment) occur before the 2050s while for others, they occur by the end of the century. This is why for higher return periods e.g., 20 years, more spread is found in the data cloud of extreme intensity anomaly as a function of additional global warming than for shorter return periods, with lower associated determination coefficient values. Hence, the timing of most extreme and rarest precipitation events remains stochastic.

To assess the trends at the local scale, we also compute a linear regression for each grid cell within Belgium (Fig. 4b). For higher return periods, some spatial variability appears with more pronounced trends for some areas of the country. Hence, the Southern flank of the Ardennian Massif as well as the northern parts of the countries show trends exceeding the Clausius-Clapeyron scaling, i.e., reaching up to 15%.K^{-1} . Those areas also show the largest frequency trends (Fig. 5b). The combination of higher atmospheric moisture and increased frequency may lead to trends exceeding 7%.K^{-1}, also called Super Clausius-Clapeyron scaling. However, the mean value in Belgium remains close to 7%.K^{-1} for the studied return levels.

Besides, concerning the trends in frequencies, we find that, the rarer the event, the higher the change in frequency (Fig. 5a). When averaged over Belgium, we estimate that for each extra degree of global warming, the 20-year return level computed over the 1981–2010 period becomes +0.6 times more frequent. This means that the 20-year return level becomes 1.6 times more frequent in a 1 degree warmer world, and 2.2 times more frequent in a 2-degree warmer world. Nevertheless, the spread of frequency anomalies increases with longer return periods, the result of the internal variability in the forcing ESMs (Fig. 5a). As for the intensities, this

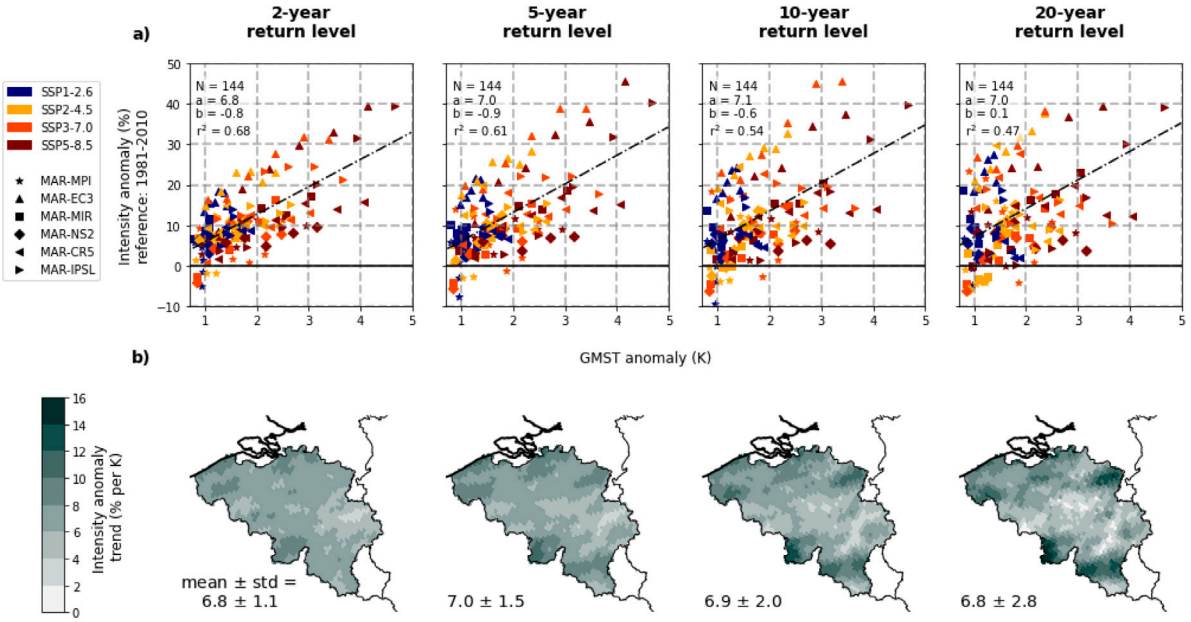

Fig. 4. (a) Intensity anomalies over 30-year moving windows relative to 1981–2010 for different return levels using the POT approach. A linear regression is applied to the data clouds (black dotted line of slope a and intercept b). (b) Same regression as in (a) but computed at each pixel location. The written values represent the map average ± the standard deviation. The results using the AM approach are very close and displayed in Supplementary Figure S4. The trends for each model are plotted on Supplementary Figure S6.

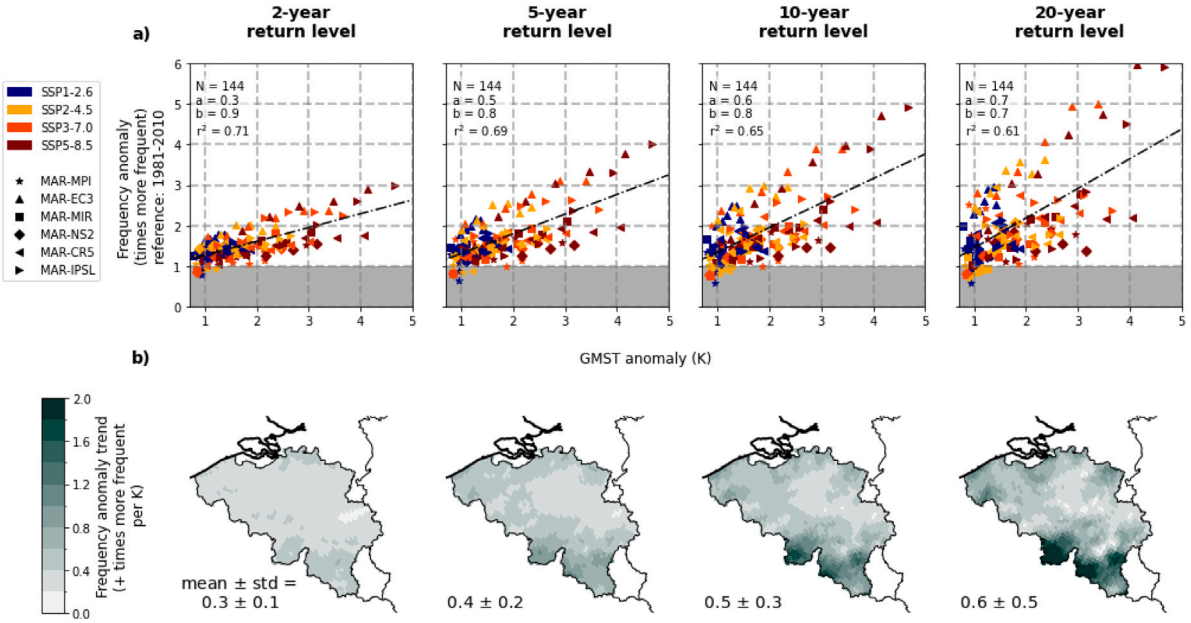

Fig. 5. (a) Frequency anomalies over 30-year moving windows relative to 1981–2010 for different return levels using the POT approach. A linear regression is applied to the data clouds (black dotted line of slope a and intercept b). (b) Same regression as in (a) but computed at each pixel location. The written values represent the map average ± the standard deviation.

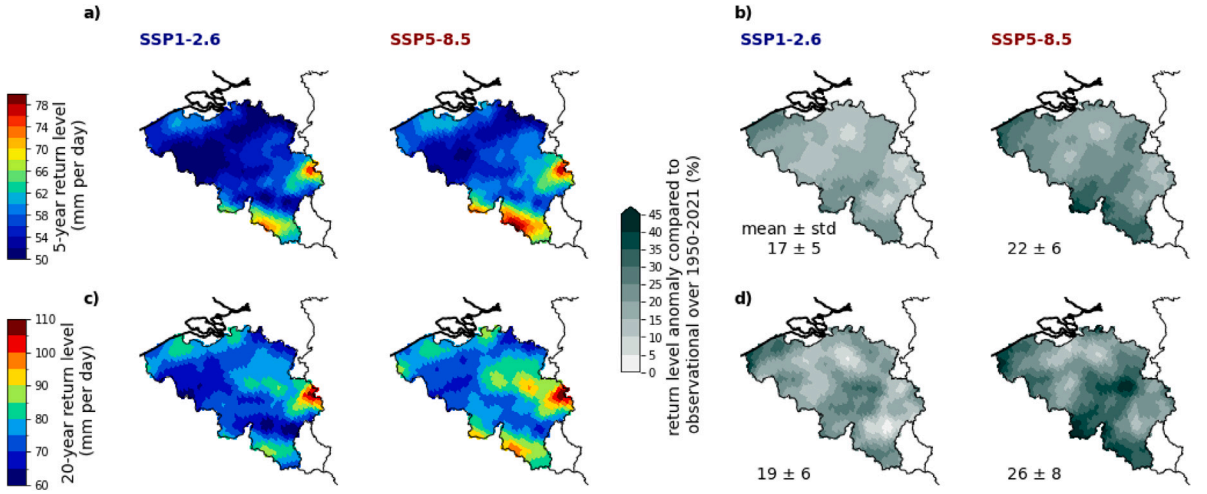

Fig. 6. (a) 5-year return level computed over 2015–2100 under SSP1-2.6 and SSP5-8.5 scenarios. (b) 5-year return anomaly as compared to 1951–2021. Same for the 20-year return level in (c) and (d). Return levels are calculated as the mean return levels of the six models (Table 1). The written values represent the map average ± the standard deviation. Widths of the 95% confidence intervals are shown in Supplementary Figure S7.

value of +0.6 times per K appears to be larger for the same specific areas, where it can easily reach + 1 times per K for the 20-year return level. This means that, in a 1-degree warmer world, the 20-year return level becomes twice as likely relative to present day.

3.2. Return levels over the whole simulated period (2015–2100)

As mentioned above, because of the internal variability of the forcing ESMs, the timing of extreme events is challenging to predict. This is why, trends are less clear for higher return periods (Figs. 4 and 5). To eliminate the effect of the internal variability, we apply an EVA to the whole future projection (2015–2100). By proceeding this way, all the simulated extreme events are accounted for in the analysis and we can estimate the absolute return level values expected within the 21st century.

When we average the obtained return level maps for the six models, and the SSP1-2.6 and 5–8.5 scenarios using the POT approach (Fig. 6), the spatial distribution of modeled extremes is equivalent to the observed one over 1951–2021. We identify two main hot-spots located on heights in the vicinity of Liège (see Fig. 1b for the location) and on the Southern flank of the Ardennian massif (Fig. 6).

Comparing the return level maps (Fig. 6) from recent observations with our future projections, the expected shift seen earlier in the anomaly analysis appears once again. On average the 20-year return level increases by 19 ± 6 and 26 ± 8% leading to return level values exceeding 100 mm per day even under a SSP1-2.6 on the precipitation hot-spot nearby the German border. This increase appears also for smaller return periods but is less pronounced, with relative increases of 17 ± 5 and 22 ± 6% for the two same scenarios. However, intensity increases are more pronounced on both Southern and Northern Flanks of The Ardennian Massif, i.e., where topographic gradients are higher. There, the increase in the 20-year return level exceeds 35% under SSP5-8.5. Low-elevated areas on the Sea-side experience similar increases.

Those more pronounced intensity shifts are linked to particularly high increases in frequency. Hence, for those areas which show the highest intensity increases, the new return period of the observational 20-year return level ranges from 4 to 7 years, even under low-emission scenarios. For the areas where the intensity increase is close to the Belgian mean, the new return period of the historical 20-year return level is of 12–15 and 8–12 years, respectively for SSP1-2.6 and SSP5-8.5 scenarios.

Fig. 6 shows maps of return levels averaged between the 6 models (Table 1). However, from one model to the other, differences can be large (Fig. 7). MAR-IPSL and MAR-EC3 display a scenario-linked logic. Hence, for those two models, the more pessimistic the emission scenario, the more extreme the return level map. Those two models also show the highest TCRs of all the ESMs forcing MAR. For the other models, the highest emission scenario does not systematically lead to the most extreme return level maps. MAR-MIR especially corroborates this statement by displaying the most extreme return level maps for the two ‘opposite’ scenarios SSP1-2.6 and SSP5-8.5 (Fig. 7), while the two intermediate scenarios display less extreme events. This implies that even under low-emission scenarios, intense extreme events will occur as well. Hence in MAR outputs, precipitation events exceeding 150 mm per day are found in all scenarios.

In terms of absolute values, MAR-EC3 yields the most intense return level-maps where the 20-year return level can reach 120 mm per day, while it only reaches 105 mm per day on the same hot-spots in MAR-NS2. However, even if MAR-NS2 return-level maps are less intense, the shift relative to observations from 1951 to 2021 remains clear, with values reaching 100 mm per day for the 20-year return level on hot-spots for all the models.

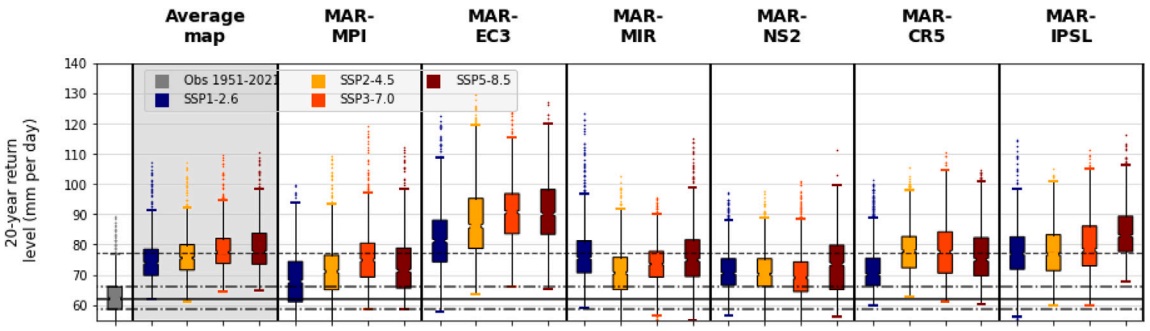

Fig. 7. Boxplots associated to the return level maps of Belgium for a return period of 20 years using all the models (Table 1) over 2015–2100. The POT approach is used for the computation of the return levels. The gray box refers to the return level map computed using observational data over 1951-2021 (Journée et al., 2023). Visual marks (horizontal black lines) have been added so each box can be compared to the observational box.

4. Discussion

4.1. Impact of the methodological choices over the EVA

Concerning the EVA, several methodological choices which might impact computed return levels are done. Hereafter, we first discuss the impact of the POT approach. Second, we look into the stationary assumption when dealing with the whole simulated period (2015–2100). Third, we discuss the bias-adjustment strategy.

4.1.1. POT approach

In this study, we also tried another common approach based on the daily precipitation annual maxima (AM), on which a Generalized Extreme Value (GEV) distribution can be fitted (Coles, 2001). This was achieved to estimate uncertainties in EVA. Concerning future anomalies in the intensity and frequency of extreme precipitation (Section 3.1.), the AM and POT approaches yield very close results (Figs. 4 and 5, and Supplementary Figure S4). This shows that our statistical methodology does not alter the effect of climate change on the intensity and frequency of extreme precipitation.

For the computation of return level absolute values over the whole simulated period (Section 3.2), AM and POT approaches show almost identical results (Fig. 8), highlighting the robustness of this study. However, in the POT approach, results would have been slightly different with lower threshold values (i.e., $u <$ 99.5th quantile). The threshold selection had to meet two main objectives. First, the chosen threshold needed to allow the POT distributions to be tailed enough to prevent underestimating higher return level values. Second, it also needed to preserve the advantage of the POT approach over the AM approach for shorter return periods, i.e., $>$ 2 selected events per year. Hence, for smaller return periods (2 to 5 years), the POT approach predicts more intense return level values. The latter approach is more reliable since it selects more events, hence providing more information about return level values associated with low return periods.

To meet these 2 conditions, several threshold values were tested based on the observational data covering 1950–2021. The 99.5 th quantile appeared to fulfill those two conditions the best, with on average over Belgium, 2.6 POT selected per year. With a lower threshold value, the risk would have been to slightly underestimate the 20-year return level intensity as compared to the AM approach which naturally leads to tailed distributions since it selects fewer events by definition (Supplementary Fig. S5).

4.1.2. Non-stationarity of the EVA

In Section 3.1, we identified trends in extreme precipitation intensity anomalies estimated using future 30-year periods. The stationary assumption usually does not hold in the presence of such trends, i.e., probability of extreme events occurrence varies in time. Here, we use a stationary approach to estimate return level values over 2015–2100 for two main reasons.

First, extreme precipitation intensity anomalies exhibit a linear trend of 7% per K, consistent with the Clausius-Clapeyron relationship, but only when data from all models are combined (Fig. 4). It is widely recognized that a multi-model ensemble mean generally provides a better estimate than each individual ensemble member (Gleckler et al., 2008; Tebaldi et al., 2011; Reichler and Kim, 2008). Hence, because of the internal variability within each ESM, trends can totally disappear when each model is considered individually, especially for higher return periods (Fig. S6).

Second, non-stationary laws were also tested for completeness, but these led to overall similar results to those of the stationary approach (Fig. 8). To incorporate non-stationarity in the POT approach, first, we make the σ of the GPD vary with the GMST anomaly. Moreover, the evolution of λ with time (Eq. (1)) can also be modeled by fitting a Poisson regression model to the distribution of the number of threshold exceedances per year (Grandry et al., 2020). By proceeding so, we model the potential non-stationarity in the number of times per year where the threshold value is exceeded. In the literature, such models are referred to as Poisson-GP models (Tramblay et al., 2013; Grandry et al., 2020). Non-stationarity can also be implemented using the AM approach by making the GEV parameters vary with the GMST anomaly. In our case, we tried a GEV model where μ and σ can vary linearly with the reached global warming level (Fig. S1).

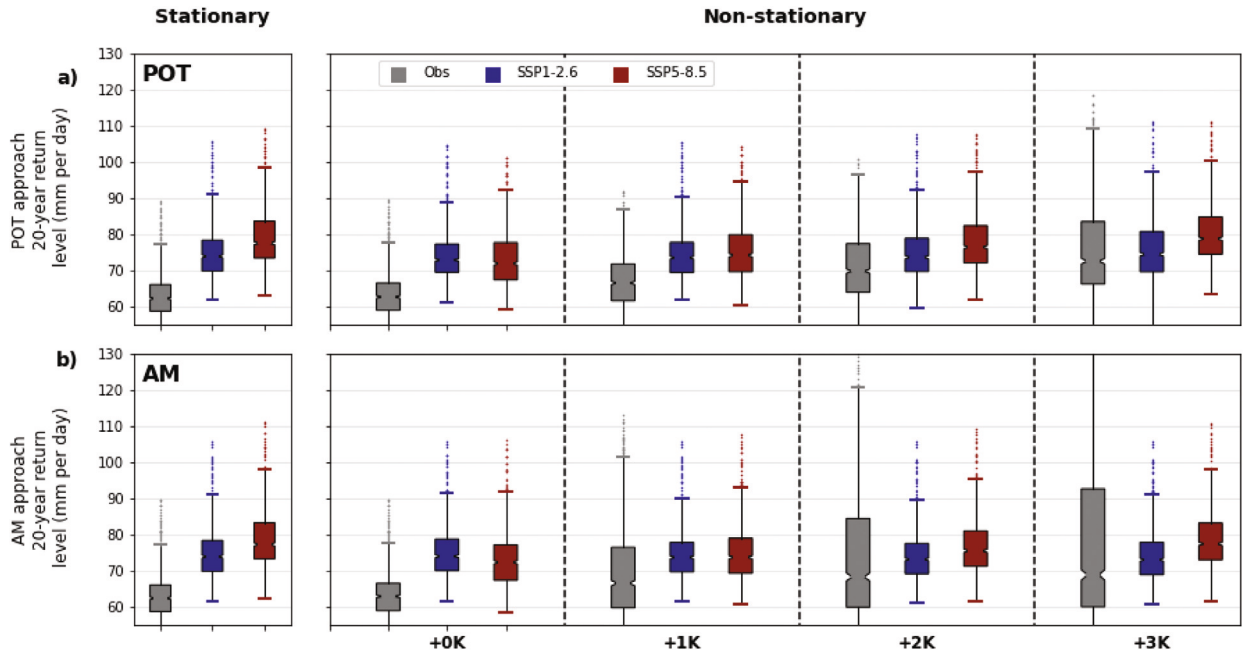

Fig. 8. Distributions of 20-year return levels using stationary and non-stationary approaches for both (a) POT and (b) AM approaches over 2015–2100. The probability of encountering extreme precipitation is time-evolving in the non-stationary approach while it is fixed in the stationary case. Return levels based on model outputs are computed as the mean of the six models (Table 1). The results of the log-ratio test, which checks whether the non-stationary approach performs better, are plotted on Supplementary Figure S8.

Non-stationary laws (GEV_n/Poisson-GP) were applied only if their performance was significantly better as compared to stationary models using the log-ratio test with a 95% confidence level (Coles, 2001).

Using non-stationary models, the difference between the 20-year return level maps under low-emission and high-emission scenario is negligible at GMST anomaly=0K, but becomes more pronounced for higher GMST anomaly values (Fig. 8). Interestingly, using observations and non-stationary approaches to extrapolate future return level values, return levels reach or even exceed the values obtained using bias-adjusted model data in some areas. This occurs when the GMST anomaly reaches 1K, specifically when using the AM approach.

However, we find that, overall, the stationary approach performs better than the non-stationary ones across most of Belgium, based on a log-ratio test (Fig S8), hence supporting our decision to base our analyses on stationary laws. We observe no significant geographical or scenario-linked patterns where and when non-stationary models perform better, and conclude that this is purely model dependent (Fig. S8). Slater et al. (2021) and Serinaldi and Kilsby (2015) have previously shown that estimating non-stationary models for precipitation comes with large uncertainties due to a small signal-to-noise ratio. Here, only one model successfully timed the most extreme precipitation events coincident with global warming, namely MAR-EC3, while for other models, predicting the timing of extreme events remains challenging.

For these reasons, fitting non-stationary laws to the data is challenging, and the stationary approach was therefore preferred in our analyses. Furthermore, the stationary approach allows us to compare future with historical return levels, since the latter were also estimated in a stationary fashion. In Section 3.2, we show average return-level maps under specific scenarios over the whole transient run. Hundhausen et al. (2024) recently suggested that proceeding this way is more appropriate due to the high internal variability within each forcing ESM. In our case, the shift in the 20-year return level values as compared to the observational ones is clear, irrespective of the model or scenario (Fig. 7). This result remains robust, particularly considering that the return periods analyzed are significantly shorter than the 85-year length of the future transient runs. However, given the variability between models, it cannot be excluded that return levels may exceed the values presented in average return level maps, especially for high-warming scenarios.

4.1.3. Bias-adjustment of extremes

To assess the potential impact of our bias-adjustment procedure on return level estimates, we computed the return levels using the POT approach over bias-adjusted MAR-ERA5 outputs (i.e, same bias-adjustment technique as presented in the paper). The return level maps are similar to the ones obtained using observational data over 1951–2021 (Fig. 9). Nevertheless, the interpolation procedure used to create the gridded observations smooths the precipitation fields, which means that associated return levels might be underestimated in some regions.

Another important result is that our bias-adjustment does not affect the impact of atmospheric warming on extremes precipitation. Hence, Figs. 3, 4 and 5 were also shown using non bias-adjusted MAR outputs, with no significant change (Supplementary Fig. S9).

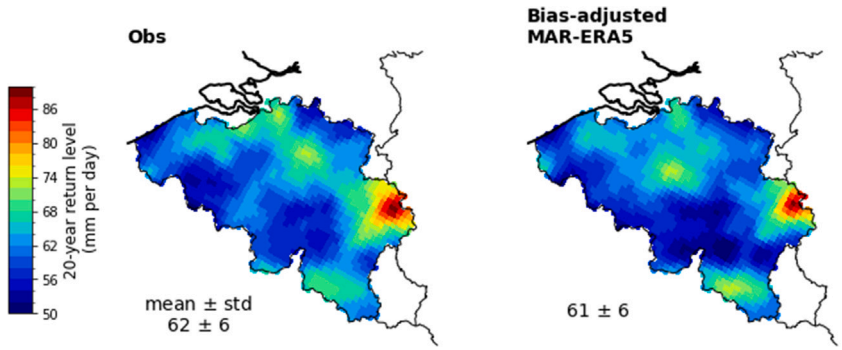

Fig. 9. 20-year return level computed using Observational data and bias-adjusted MAR-ERA5 data over 1951–2021. The POT approach is used here for the computation of the return levels. The written values represent the map average ± the standard deviation.

4.2. Implication of the results

In our results, we show that the average trend for extreme intensity in Belgium follows the Clausius-Clapeyron scaling of 7%.K^{-1} . This increase is linked to a clear shift towards higher values of the distributions modes (u of the GPD under the POT approach) and spreads (σ parameter) (Fig. 3). In areas showing higher topographic gradients in the South, and on the sea-side, for higher return levels, the intensity and frequency trends appear to be up to twice larger than the average over Belgium (Figs. 4 and 5). This suggests that even at small spatial scales, the impact of global warming on both the intensity and frequency of extreme precipitation might vary significantly, although statistical noise may hamper strong conclusions at such scales. This result is in line with Ludwig et al. (2023) and Hundhausen et al. (2024) who found extreme precipitation intensity increases following the Clausius-Clapeyron scaling or even beyond it in Western Germany.

Hot-spots of extreme precipitation have been clearly identified in our analysis. Sensitive areas appear in the vicinity of the city of Liège (Vesdre watershed) on the highest parts of the country, which were highly impacted by the July 2021 event (Fig. 1) . There, 20-year return levels can reach 110 mm per day irrespective of the scenario. Additional hot-spots appear in the future (Fig. 6). The southern flank of the Ardennian Massif experiences high return level values and this hot-spot especially stands out when it comes to lower return periods (e.g. 2 or 5 years). This indicates that the associated extreme precipitation distributions at these locations are spread but with lighter tails, i.e., with smaller ξ parameter values than in the above mentioned hot-spot. Yet, some other extreme-prone areas appear also at lower elevations, notably around the city of Antwerpen (Fig. 1). There, extreme precipitation values are necessarily linked to other factors than topography given the flatness of the area. Compared to observational return levels computed over 1951–2021, intensity increases can reach up to 40% (Fig. 7), which is even higher than the projected change over North-Western Europe under high-emission scenarios (20%–35%) (Rajczak and Schär, 2017).

4.3. Limitations of the study

MAR underestimates extremes (Table 2, Fig. 2), especially for low-elevated Belgium where (Doutreloup et al., 2019) previously showed that MAR tends to underestimate convective precipitation, supporting the need for bias-adjustment. For bias-adjustment, we use a probabilistic approach based on distributions (Teutschbein and Seibert, 2012). However, in the coastal area north of the city of Ghent (Fig. 1), the underestimation of extreme quantiles in MAR (Fig. 2) is such that the estimated return levels here might not be realistic. Moreover, only one RCM is used, while Hosseinzadehtalaei et al. (2018) showed that the largest source of uncertainty lies in the RCMs themselves followed by the ESMs forcing at their limits.

Our analyses are conducted on daily basis because RCMs tend to underestimate hourly peaks of extreme precipitation (Pichelli et al., 2021; Ban et al., 2021). Extreme precipitation underestimation may possibly originate from the hydrostatic hypothesis in MAR, but Malardel (2014) showed that with an adequate parametrization of convection, RCMs perform well at spatial resolutions > 3 km. Moreover, MAR is run using a single nesting procedure over a small domain. Due to the small area of the domain and the relatively coarse resolution of the forcing ESMs (between 40 and 130 km), the underestimation of extreme precipitation might result from the fact that realistic convective cells do not develop (Brisson et al., 2016). However, Wyard et al. (2018), showed that the different resolutions of forcing fields do not have a major impact on RCMs outputs such as the simulated cloud cover in Belgium. Future sensitivity analyses should investigate the impact of spatial resolution on precipitation in Belgium.

Finally, the impact of climate change can largely vary depending on the future period and model selected (Figs. 4a and 7). Future work should assess the ability of the forcing ESMs to model extreme weather patterns over Western Europe. For instance, examining extreme weather types at a synoptic scale in CMIP6 ESMs outputs might be an option. Model differences may not only be explained by their different TCRs, but also by their ability to simulate the frequency of Cut-off lows and other variables as well. Using analogues, Thompson et al. (2024) suggested that the frequency and persistence of synoptic weather cut-off lows, similar to July 2021, show an increasing trend in Northern-Western Europe. Insua-Costa et al. (2022) showed that the July 2021 event itself was particularly intense due to the huge moisture content in the atmosphere caused by massive prior evapotranspiration from

Western European forests. Using MAR outputs and ESM data, we could identify which weather patterns lead to the most intense precipitation events in Belgium. Building on this, we could test whether the ESMs used in this study predict coherent extreme weather frequencies.

5. Conclusion

In this study, we estimate projected trends in extreme precipitation frequency and intensity over Belgium. The Regional Climate Model MAR forced by six CMIP6 ESMs at 5 km resolution shows that the intensity of future extreme precipitation will, on average over the country, increase following the Clausius Clapeyron scaling of 7% per added degree of global warming. However, MAR projects larger trends for frequency anomalies over specific areas, suggesting that intensity increase may locally exceed the Clausius Clapeyron scaling, i.e, super Clausius Clapeyron scaling, notably in high topographic gradient areas and in low-elevated coastal areas.

When bias-adjusted, MAR outputs show return level values associated to a 20-year return period reaching 100 mm per day or more in extreme precipitation hot-spots throughout the 21st century. Projected intensity increases can reach up to 40% under high-emission scenarios.

Our study identifies Belgian areas that are at risk of experiencing more frequent extreme precipitation events, notably the Ardennian Massif and low-elevated coastal areas. We do not cover hydrological extremes, such as floods, for which impact studies might be conducted using bias-adjusted MAR outputs and hydrological models. Future work should identify climate drivers that enhance the strength and frequency of extreme events.

CRediT authorship contribution statement

Josip Brajkovic: Writing – original draft, Methodology, Formal analysis, Conceptualization. **Xavier Fettweis:** Writing – original draft, Supervision, Data curation. **Brice Noël:** Writing – original draft. **Hans Van De Vyver:** Supervision. **Nicolas Ghilain:** Writing – original draft, Supervision, Data curation. **Pierre Archambeau:** Writing – original draft, Supervision. **Michel Pirotton:** Supervision. **Sébastien Doutreloup:** Writing – original draft, Supervision.

Credits

This study has been funded under the Brain program of the Belgian Science Policy through the Cordex.BeII research project (CONTRACT NR B2/223/P1/CORDEX.be II). Computational resources used to perform MAR simulations have been provided by the Consortium des Équipements de Calcul Intensif (CÉCI), funded by F.R.S.-FNRS, Belgium under Grant No. 2.5020.11 and the Tier-1 supercomputer (Zenobe) of the Fédération Wallonie Bruxelles infrastructure funded by the Walloon Region under Grant Agreement No. 1117545.

Declaration of competing interest

The authors declare that they have no known competing financial interests or personal relationships that could have appeared to influence the work reported in this paper.

Appendix A. Supplementary data

Supplementary material related to this article can be found online at https://doi.org/10.1016/j.ejrh.2025.102399.

Data availability

Data will be made available on request.

References

Arnbjerg-Nielsen, K., 2012. Quantification of climate change effects on extreme precipitation used for high resolution hydrologic design. Urban Water J. 9 (2), 57–65. http://dx.doi.org/10.1080/1573062x.2011.630091.

Babaousmail, H., Hou, R., Ayugi, B., Sian, K.T.C.L.K., Ojara, M., Mumo, R., Chehbouni, A., Ongoma, V., 2022. Future changes in mean and extreme precipitation over the Mediterranean and Sahara regions using bias-corrected CMIP6 models. Int. J. Climatol. 42 (14), 7280–7297. http://dx.doi.org/10.1002/joc.7644, arXiv:https://rmets.onlinelibrary.wiley.com/doi/pdf/10.1002/joc.7644, URL: https://rmets.onlinelibrary.wiley.com/doi/abs/10.1002/joc.7644.

Ban, N., Caillaud, C., Coppola, E., Pichelli, E., Sobolowski, S., Adinolfi, M., Ahrens, B., Alias, A., Anders, I., Bastin, S., Belušić, D., Berthou, S., Brisson, E., Cardoso, R., Chan, S., Christensen, O., Fernández, J., Fita, L., Frisius, T., Zander, M., 2021. The first multi-model ensemble of regional climate simulations at kilometer-scale resolution, part I: evaluation of precipitation. Clim. Dyn. 57, http://dx.doi.org/10.1007/s00382-021-05708-w.

Bechtold, P., Bazile, E., Guichard, F., Mascart, P., Richard, E., 2001. A mass-flux convection scheme for regional and global models. Q. J. R. Meteorol. Soc. 127 (573), 869–886. http://dx.doi.org/10.1002/qj.49712757309, arXiv:https://rmets.onlinelibrary.wiley.com/doi/pdf/10.1002/qj.49712757309, URL: https://rmets.onlinelibrary.wiley.com/doi/abs/10.1002/qj.49712757309.

Brisson, E., Demuzere, M., van Lipzig, N.P., 2016. Modelling strategies for performing convection-permitting climate simulations. Meteorol. Z. 25 (2), 149–163. http://dx.doi.org/10.1127/metz/2015/0598.

Coles, S., 2001. An introduction to statistical modeling of extreme values. In: Springer Series in Statistics, Springer-Verlag, London.

Cunnane, C., 1979. A note on the Poisson assumption in partial duration series models. Water Resour. Res. 15 (2), 489–494. http://dx.doi.org/10.1029/WR015i002p00489, arXiv:https://agupubs.onlinelibrary.wiley.com/doi/pdf/10.1029/WR015i002p00489, URL: https://agupubs.onlinelibrary.wiley.com/doi/abs/10.1029/WR015i002p00489.

de Vyver, H.V., Schaeybroeck, B.V., Troch, R.D., Cruz, L.D., Hamdi, R., Villanueva-Birriel, C., Marbaix, P., van Ypersele, J.-P., Wouters, H., Broucke, S.V., van Lipzig, N.P.M., Doutreloup, S., Wyard, C., Scholzen, C., Fettweis, X., Caluwaerts, S., Termonia, P., 2021. Evaluation framework for subdaily rainfall extremes simulated by regional climate models. J. Appl. Meteorol. Clim. 60 (10), 1423–1442. http://dx.doi.org/10.1175/JAMC-D-21-0004.1, URL: https://journals.ametsoc.org/view/journals/apme/60/10/JAMC-D-21-0004.1.xml.

Dewals, B., Erpicum, S., Pirotton, M., Archambeau, P., 2021. Extreme floods in Belgium. The July 2021 extreme floods in the Belgian part of the Meuse basin. Hydrolink (2021/4), 104, https://hdl.handle.net/20.500.11970/109527 and https://www.iahr.org/library/hydrolink?hid=412.

Doutreloup, S., Bois, B., Pohl, B., Zito, S., Richard, Y., 2022a. Climatic comparison between Belgium, Champagne, Alsace, Jura and Bourgogne for wine production using the regional model MAR. OENO One 56 (3), http://dx.doi.org/10.20870/oeno-one.2022.56.3.5356, URL: https://oeno-one.eu/article/view/5356#.

Doutreloup, S., Fettweis, X., Rahif, R., Elnagar, E., Pourkiaei, M.S., Amaripadath, D., Attia, S., 2022b. Historical and future weather data for dynamic building simulations in Belgium using the regional climate model MAR: typical and extreme meteorological year and heatwaves. Earth Syst. Sci. Data 14 (7), 3039–3051. http://dx.doi.org/10.5194/essd-14-3039-2022, URL: https://essd.copernicus.org/articles/14/3039/2022/.

Doutreloup, S., Wyard, C., Amory, C., Kittel, C., Erpicum, M., Fettweis, X., 2019. Sensitivity to convective schemes on precipitation simulated by the regional climate model MAR over Belgium (1987–2017). Atmosphere 10 (1), http://dx.doi.org/10.3390/atmos10010034, URL: https://www.mdpi.com/2073-4433/10/1/34.

ECMWF, 2021. Extreme rain in Germany and Belgium in July 2021. URL: https://www.ecmwf.int/en/newsletter/169/news/extreme-rain-germany-and-belgium-july-2021.

Erpicum, M., Nouri, M., Demoulin, A., 2017. The climate of Belgium and Luxembourg. In: Landscapes and Landforms of Belgium and Luxembourg. Springer International Publishing, pp. 35–41. http://dx.doi.org/10.1007/978-3-319-58239-9_3.

Fettweis, X., Wyard, C., Doutreloup, S., Belleflamme, A., 2017. Noël 2010 en Belgique : neige en Flandre et pluie en Haute-Ardenne. Bull. de la SociétÉ Géographique de Liège 68, http://dx.doi.org/10.25518/0770-7576.4568, arXiv:https://rmets.onlinelibrary.wiley.com/doi/pdf/10.1002/joc.4879, URL: https://rmets.onlinelibrary.wiley.com/doi/abs/10.1002/joc.4879.

Gallée, H., 1995. Simulation of the mesocyclonic activity in the Ross Sea, Antarctica. Mon. Weather Rev. 123 (7), 2051–2069. http://dx.doi.org/10.1175/1520-0493(1995)123<2051:SOTMAI>2.0.CO;2, URL: https://journals.ametsoc.org/view/journals/mwre/123/7/1520-0493_1995_123_2051_sotmai_2_0_co_2.xml.

Gallée, H., Schayes, G., 1994a. Development of a three-dimensional Meso-γ primitive equation model: Katabatic winds simulation in the area of Terra Nova Bay, Antarctica. Mon. Weather Rev. 122 (4), 671–685. http://dx.doi.org/10.1175/1520-0493(1994)122<0671:DOATDM>2.0.CO;2, URL: https://journals.ametsoc.org/view/journals/mwre/122/4/1520-0493_1994_122_0671_doatdm_2_0_co_2.xml.

Gallée, H., Schayes, G., 1994b. Development of a three-dimensional Meso-γ primitive equation model: Katabatic winds simulation in the area of Terra Nova Bay, Antarctica. Mon. Weather Rev. 122 (4), 671–685. http://dx.doi.org/10.1175/1520-0493(1994)122<0671:DOATDM>2.0.CO;2, URL: https://journals.ametsoc.org/view/journals/mwre/122/4/1520-0493_1994_122_0671_doatdm_2_0_co_2.xml.

Gilleland, E., 2003. Ismev: An introduction to statistical modeling of extreme values. URL: https://cran.r-project.org/web/packages/ismev, R package version 1.42.

Gleckler, P.J., Taylor, K.E., Doutriaux, C., 2008. Performance metrics for climate models. J. Geophys. Res.: Atmospheres 113 (D6), http://dx.doi.org/10.1029/2007jd008972.

Grailet, J.-F., Hogan, R.J., Ghilain, N., Fettweis, X., Grégoire, M., 2024. Inclusion of the ECMWF ecRad radiation scheme (v1.5.0) in the MAR model (v3.14), regional evaluation for Belgium and assessment of surface shortwave spectral fluxes at uccle observatory. EGUsphere 2024, 1–33. http://dx.doi.org/10.5194/egusphere-2024-1858, URL: https://egusphere.copernicus.org/preprints/2024/egusphere-2024-1858/.

Grandry, M., Gailliez, S., Brostaux, Y., Degré, A., 2020. Looking at trends in high flows at a local scale: The case study of Wallonia (Belgium). J. Hydrol.: Reg. Stud. 31, 100729. http://dx.doi.org/10.1016/j.ejrh.2020.100729, URL: https://www.sciencedirect.com/science/article/pii/S2214581820302032.

Gründemann, G., van de Giesen, N., Brunner, L., Ent, R., 2022. Rarest rainfall events will see the greatest relative increase in magnitude under future climate change. Commun. Earth Environ. 3, http://dx.doi.org/10.1038/s43247-022-00558-8.

Hosseinzadehtalaei, P., Tabari, H., Willems, P., 2018. Precipitation intensity–duration–frequency curves for central Belgium with an ensemble of EURO-CORDEX simulations, and associated uncertainties. Atmos. Res. 200, 1–12. http://dx.doi.org/10.1016/j.atmosres.2017.09.015, URL: https://www.sciencedirect.com/science/article/pii/S0169809516303428.

Hundhausen, M., Feldmann, H., Kohlhepp, R., Pinto, J.G., 2024. Climate change signals of extreme precipitation return levels for Germany in a transient convection-permitting simulation ensemble. Int. J. Climatol. 44 (5), 1454–1471. http://dx.doi.org/10.1002/joc.8393, arXiv:https://rmets.onlinelibrary.wiley.com/doi/pdf/10.1002/joc.8393, URL: https://rmets.onlinelibrary.wiley.com/doi/abs/10.1002/joc.8393.

Insua-Costa, D., Senande-Rivera, M., Llasat, M.C., Miguez-Macho, G., 2022. The central role of forests in the 2021 European floods. Environ. Res. Lett. 17 (6), 064053. http://dx.doi.org/10.1088/1748-9326/ac6f6b.

IPCC, 2023a. Climate Change 2021 – The Physical Science Basis: Working Group I Contribution to the Sixth Assessment Report of the Intergovernmental Panel on Climate Change. Cambridge University Press.

IPCC, 2023b. Global carbon and other biogeochemical cycles and feedbacks. In: Climate Change 2021 – the Physical Science Basis: Working Group I Contribution To the Sixth Assessment Report of the Intergovernmental Panel on Climate Change. Cambridge University Press, pp. 673–816.

Jain, S., Scaife, A., Shepherd, T., Deser, C., Dunstone, N., Schmidt, G., Trenberth, K., Turkington, T., 2023. Importance of internal variability for climate model assessment. Npj Clim. Atmos. Sci. 6, http://dx.doi.org/10.1038/s41612-023-00389-0.

Journée, M., Goudenhoofdt, E., Vannitsem, S., Delobbe, L., 2023. Quantitative rainfall analysis of the 2021 mid-July flood event in Belgium. EGUsphere 2023, 1–24. http://dx.doi.org/10.5194/egusphere-2023-542, URL: https://egusphere.copernicus.org/preprints/2023/egusphere-2023-542/.

Kendon, E.J., Fischer, E.M., Short, C.J., 2023. Variability conceals emerging trend in 100yr projections of UK local hourly rainfall extremes. Nat. Commun. 14 (1), http://dx.doi.org/10.1038/s41467-023-36499-9.

Kreienkamp, F., Philip, S.Y., Tradowsky, J.S., Kew, S.F., Lorenz, P., Arrighi, J., Belleflamme, A., Bettmann, T., Caluwaerts, S., Chan, S.C., Ciavarella, A., De Cruz, L., de Vries, H., Demuth, N., Ferrone, A., Fischer, r.M., Fowler, H.J., Goergen, K., Heinrich, D., Henrichs, Y., Lenderink, G., Kaspar, F., Nilson, E., Otto, F.E.L., Ragone, F., Seneviratne, S.I., Singh, R.K., Skålevåg, A., Termonia, P., Thalheimer, L., van Aalst, M., Van den Bergh, J., Van de Vyver, H., Vannitsem, S., van Oldenborgh, G.J., Van Schaeybroeck, B., Vautard, R., Vonk, D., Wanders, N., 2021. Rapid attribution of heavy rainfall events leading to the severe flooding in Western Europe during July 2021. In: World Weather Atribution, p. 51.

Ludwig, P., Ehmele, F., Franca, M.J., Mohr, S., Caldas-Alvarez, A., Daniell, J.E., Ehret, U., Feldmann, H., Hundhausen, M., Knippertz, P., Küpfer, K., Kunz, M., Mühr, B., Pinto, J.G., Quinting, J., Schäfer, A.M., Seidel, F., Wisotzky, C., 2023. A multi-disciplinary analysis of the exceptional flood event of July 2021 in central Europe – Part 2: Historical context and relation to climate change. Nat. Hazards Earth Syst. Sci. 23 (4), 1287–1311. http://dx.doi.org/10.5194/nhess-23-1287-2023, URL: https://nhess.copernicus.org/articles/23/1287/2023/.

Luppichini, M., Bini, M., Giannecchini, R., Zanchetta, G., 2023. High-resolution spatial analysis of temperature influence on the rainfall regime and extreme precipitation events in north-central Italy. Sci. Total Environ. 880, 163368. http://dx.doi.org/10.1016/j.scitotenv.2023.163368.

Malardel, S., 2014. Physics/dynamics Coupling at Very High Resolution: Permitted Versus Parametrized Convection (Ph.D. thesis). ECMWF, ECMWF, Shinfield Park, Reading, Shinfield Park, Reading, pp. 83–98.

Mohr, S., Ehret, U., Kunz, M., Ludwig, P., Caldas-Alvarez, A., Daniell, J.E., Ehmele, F., Feldmann, H., Franca, M.J., Gattke, C., Hundhausen, M., Knippertz, P., Küpfer, K., Mühr, B., Pinto, J.G., Quinting, J., Schäfer, A.M., Scheibel, M., Seidel, F., Wisotzky, C., 2023. A multi-disciplinary analysis of the exceptional flood event of July 2021 in central Europe – Part 1: Event description and analysis. Nat. Hazards Earth Syst. Sci. 23 (2), 525–551. http://dx.doi.org/10.5194/nhess-23-525-2023, URL: https://nhess.copernicus.org/articles/23/525/2023/.

Muñoz Lopez, C., Wang, L.-P., Willems, P., 2023. Statistical characterization of rainfall fields based upon a 12-year high-resolution radar archive of Belgium. Atmos. Res. 283, 106544. http://dx.doi.org/10.1016/j.atmosres.2022.106544, URL: https://www.sciencedirect.com/science/article/pii/S0169809522005300.

Pfahl, S., O'Gorman, P.A., Fischer, E.M., 2017. Understanding the regional pattern of projected future changes in extreme precipitation. Nat. Clim. Chang. 7 (6), 423–427. http://dx.doi.org/10.1038/nclimate3287.

Pichelli, E., Coppola, E., Sobolowski, S.P., Ban, N., Giorgi, F., Stocchi, P., Alias, A., Belušić, D., Berthou, S., Caillaud, C., Cardoso, R.M., Chan, S.C., Christensen, O.B., Dobler, A.H., de Vries, H., Goergen, K., Kendon, E.J., Keuler, K., Lenderink, G., Lorenz, T., Mishra, A.N., Panitz, H.-J., Schär, C.M., Soares, P.M.M., Truhetz, H., Vergara-Temprado, J., 2021. The first multi-model ensemble of regional climate simulations at kilometer-scale resolution part 2: historical and future simulations of precipitation. Clim. Dyn. 56, 3581–3602, URL: https://api.semanticscholar.org/CorpusID:231747484.

Pierce, D.W., Cayan, D.R., Maurer, E.P., Abatzoglou, J.T., Hegewisch, K.C., 2015. Improved bias correction techniques for hydrological simulations of climate change. J. Hydrometeorol. 16 (6), 2421–2442. http://dx.doi.org/10.1175/JHM-D-14-0236.1, URL: https://journals.ametsoc.org/view/journals/hydr/16/6/jhm-d-14-0236_1.xml.

Rajczak, J., Schär, C., 2017. Projections of future precipitation extremes over Europe: A multimodel assessment of climate simulations. J. Geophys. Res.: Atmospheres 122 (20), 10,773–10,800. http://dx.doi.org/10.1002/2017JD027176, arXiv:https://agupubs.onlinelibrary.wiley.com/doi/pdf/10.1002/2017JD027176, URL: https://agupubs.onlinelibrary.wiley.com/doi/abs/10.1002/2017JD027176.

Reichler, T., Kim, J., 2008. How well do coupled models simulate today's climate? Bull. Am. Meteorol. Soc. 89 (3), 303–312. http://dx.doi.org/10.1175/bams-89-3-303.

Serinaldi, F., Kilsby, C.G., 2015. Stationarity is undead: Uncertainty dominates the distribution of extremes. Adv. Water Resour. 77, 17–36. http://dx.doi.org/10.1016/j.advwatres.2014.12.013.

Slater, L.J., Anderson, B., Buechel, M., Dadson, S., Han, S., Harrigan, S., Kelder, T., Kowal, K., Lees, T., Matthews, T., Murphy, C., Wilby, R.L., 2021. Nonstationary weather and water extremes: a review of methods for their detection, attribution, and management. Hydrol. Earth Syst. Sci. 25 (7), 3897–3935. http://dx.doi.org/10.5194/hess-25-3897-2021.

Sobolowski, S., Somot, S., Fernandez, J., Evin, G., Maraun, D., Kotlarski, S., Jury, M., Benestad, R.E., Teichmann, C., Christensen, O.B., Katharina, B., Buonomo, E., Katragkou, E., Steger, C., Sørland, S., Nikulin, G., McSweeney, C., Dobler, A., Palmer, T., Wilke, R., Boé, J., Brunner, L., Ribes, A., Qasmi, S., Nabat, P., Sevault, F., Oudar, T., Brands, S., 2023. EURO-CORDEX CMIP6 GCM Selection & Ensemble Design: Best Practices and Recommendations. http://dx.doi.org/10.5281/zenodo.7673400, Zenodo, URL: https://doi.org/10.5281/zenodo.7673400.

Taesombut, V., Yevjevich, V.M., et al., 1978. Use of Partial Flood Series for Estimating Distribution of Maximum Annual Flood Peak. Colorado State University Fort Collins, CO.

Tebaldi, C., Arblaster, J.M., Knutti, R., 2011. Mapping model agreement on future climate projections: Mapping model agreement. Geophys. Res. Lett. 38 (23), http://dx.doi.org/10.1029/2011gl049863.

Teutschbein, C., Seibert, J., 2012. Bias correction of regional climate model simulations for hydrological climate-change impact studies: Review and evaluation of different methods. J. Hydrol. 456–457, 12–29. http://dx.doi.org/10.1016/j.jhydrol.2012.05.052, URL: https://www.sciencedirect.com/science/article/pii/S0022169412004556.

Thompson, V., Coumou, Philip, S., Kew, S., Pinto, I., 2024. Attribution using analogues: a case study of the Western European flood event of July 2021. http://dx.doi.org/10.5194/egusphere-egu24-1716, EGU General Assembly 2024, Vienna, Austria, 14–19 Apr 2024.

Tradowsky, J.S., Philip, S.Y., Kreienkamp, F., Kew, S.F., Lorenz, P., Arrighi, J., Bettmann, T., Caluwaerts, S., Chan, S.C., De Cruz, L., de Vries, H., Demuth, N., Ferrone, A., Fischer, E.M., Fowler, H.J., Goergen, K., Heinrich, D., Henrichs, Y., Kaspar, F., Lenderink, G., Nilson, E., Otto, F.E.L., Ragone, F., Seneviratne, S.I., Singh, R.K., Sk° alevåg, A., Termonia, P., Thalheimer, L., van Aalst, M., Van den Bergh, J., Van de Vyver, H., Vannitsem, S., van Oldenborgh, G.J., Van Schaeybroeck, B., Vautard, R., Vonk, D., Wanders, N., 2023. Attribution of the heavy rainfall events leading to severe flooding in Western Europe during July 2021. Climatic Change 176 (7), 38.

Tramblay, Y., Neppel, L., Carreau, J., Najib, K., 2013. Non-stationary frequency analysis of heavy rainfall events in southern France. Hydrol. Sci. J. 58 (2), 280–294. http://dx.doi.org/10.1080/02626667.2012.754988.

Trenberth, K.E., Dai, A., Rasmussen, R.M., Parsons, D.B., 2003. The changing character of precipitation. Bull. Am. Meteorol. Soc. 84 (9), 1205–1218. http://dx.doi.org/10.1175/bams-84-9-1205.

Wyard, C., Doutreloup, S., Belleflamme, A., Wild, M., Fettweis, X., 2018. Global radiative flux and cloudiness variability for the period 1959–2010 in Belgium: A comparison between reanalyses and the regional climate model MAR. Atmosphere 9 (7), http://dx.doi.org/10.3390/atmos9070262, URL: https://www.mdpi.com/2073-4433/9/7/262.

Wyard, C., Scholzen, C., Doutreloup, S., Hallot, E., Fettweis, X., 2021. Future evolution of the hydroclimatic conditions favouring floods in the south-east of Belgium by 2100 using a regional climate model. Int. J. Climatol. 41 (1), 647–662. http://dx.doi.org/10.1002/joc.6642, arXiv:https://rmets.onlinelibrary.wiley.com/doi/pdf/10.1002/joc.6642, URL: https://rmets.onlinelibrary.wiley.com/doi/abs/10.1002/joc.6642.

Wyard, C., Scholzen, C., Fettweis, X., Van Campenhout, J., François, L., 2017. Decrease in climatic conditions favouring floods in the south-east of Belgium over 1959–2010 using the regional climate model MAR. Int. J. Climatol. 37 (5), 2782–2796. http://dx.doi.org/10.1002/joc.4879, arXiv:https://rmets.onlinelibrary.wiley.com/doi/pdf/10.1002/joc.4879, URL: https://rmets.onlinelibrary.wiley.com/doi/abs/10.1002/joc.4879.